Applied Catalysis B: Environmental 125 (2012) 172–179

Contents lists available at SciVerse ScienceDirect

Applied Catalysis B: Environmental

journal homepage: www.elsevier.com/locate/apcatb

Enhanced selective hydrodechlorination of 1,2-dichloroethane to ethylene on Pt–Ag/TiO_2 catalysts prepared by sequential photodeposition

Yuxiang Han, Juan Zhou, Wenjuan Wang, Haiqin Wan*, Zhaoyi Xu, Shourong Zheng*, Dongqiang Zhu

State Key Laboratory of Pollution Control and Resource Reuse, Jiangsu Key Laboratory of Vehicle Emissions Control, School of the Environment, Nanjing University, Nanjing 210046, China

ARTICLE INFO

Article history:
Received 9 January 2012
Received in revised form 17 May 2012
Accepted 19 May 2012
Available online 27 May 2012

Keywords:
Catalytic hydrodechlorination
1,2-Dichloroethane
Ethylene selectivity
Pt–Ag/TiO_2 catalyst
Sequential photodeposition

ABSTRACT

TiO_2 supported Pt–Ag bimetallic catalysts were prepared using a sequential photodeposition method (denoted as *pd*-Pt–Ag/TiO_2). For comparison, supported bimetallic catalysts were also prepared using the conventional impregnation method (denoted as *im*-Pt–Ag/TiO_2). The catalysts were characterized by X-ray diffraction, transition electron microscopy, CO chemisorption, IR spectroscopy of CO adsorption, and X-ray photoelectron spectroscopy. Characterization results indicated that photodeposition led to site-specific deposition of metallic Ag domain on the surface of Pt particles and thus to the formation of core–shell (Pt@Ag) like bimetallic species, which effectively blocked the adjacent Pt sites. However, Pt–Ag ensemble was predominant in *im*-Pt–Ag/TiO_2. Accordingly, hydrodechlorination of 1,2-dichloroethane exhibited substantially higher ethylene selectivity and catalytic stability on *pd*-Pt–Ag/TiO_2 than on *im*-Pt–Ag/TiO_2 at similar Ag loading levels. Findings from this study highlight the potential of using sequentially photodeposited core–shell like bimetallic catalysts to enhance the ethylene selectivity in hydrodechlorination of 1,2-dichloroethane.

1. Introduction

Due to the strong mutagenic and carcinogenic activities, chlorinated hydrocarbons are highly toxic volatile pollutants [1,2]. The release of chlorinated hydrocarbons to the atmospheric environment is one of the major causes of ozone depletion and global warming [3,4]. Catalytic hydrodechlorination (HDC) provides a cost-effective and non-destructive approach to convert chlorinated hydrocarbons into valuable hydrocarbons that could be recovered for commercial use [5–8].

For the HDC of chlorinated hydrocarbons, monometallic catalysts from group VIII are active but not selective. For example, in the HDC of 1,2-dichloroethane ethane is the dominant product on supported monometallic Pt or Pd catalysts due to the strong adsorption ability for ethylene (intermediate product) and the high catalytic hydrogenation activity [9,10]. Ethylene selectivity in the HDC of 1,2-dichloroethane can be improved substantially by adding a second metal from group IB to tune the properties of the superficial metal [11–19]. The enhanced selectivity of the supported bimetallic catalyst can be well explained in terms of the ensemble/geometric effect, by which the surface noble metal atoms are effectively isolated by the second metal due to dilution effect. As a result, the second metal serves as the active sites for dechlorination of 1,2-dichloroethane, and the noble metal serves as the active sites for H_2 activation to regenerate the deactivated second metal.

The ethylene selectivity in the catalytic HDC of 1,2-dichloroethane is highly dependent on the methodology for preparation of the supported bimetallic catalyst. For example, Rhodes et al. [12] synthesized a bimetallic Pt–Sn catalyst on SiO_2 using a method of controlled surface reaction and observed enhanced initial ethylene selectivity compared with the catalyst prepared by the impregnation method. Luebke et al. [20] reported that the ethylene selectivity positively correlated to the bimetallic alloy content in Pt–Cu/C. Heinrichs et al. [16] prepared SiO_2 supported bimetallic catalysts with complete accessibility of sinter-proof metal particles using the sol–gel method. Xie et al. [10] found that a more precise control of the structure of the bimetallic alloy in Pt–Cu/SiO_2 could be achieved by using poly(amidoamine) dendrimer metal nanocomposites as the precursor.

Photodeposition provides an alternative approach for preparing supported metal catalyst having highly dispersed active sites [21–23]. In principle, the aqueous metal ions can be readily reduced by photo-induced electrons when they are excited from the valence band to the conduction band of a semiconductor (e.g. TiO_2) upon light irradiation; as a result, metallic particles are deposited on the surface of the semiconductor [24–26]. It is interesting to note that for Pt/TiO_2 surface Pt particle can serve as a sink of photo-induced electrons due to the high work function [27,28]. Hence,

* Corresponding authors. Tel.: +86 25 89680373; fax: +86 25 89680596.
E-mail addresses: wanhq@nju.edu.cn (H. Wan), srzheng@nju.edu.cn (S. Zheng).

0926-3373/$ – see front matter © 2012 Elsevier B.V. All rights reserved.
http://dx.doi.org/10.1016/j.apcatb.2012.05.016

during the synthesis process of bimetallic catalysts reduction of the second-metal ions (such as Ag^+) would preferentially occur on the surface of Pt particles, leading to site specific deposition of the second metal on the surface of Pt particles. It should be emphasized that the ethylene selectivity in the HDC of 1,2-dichloroethane is positively correlated to the enrichment of second metal in supported bimetallic catalyst. Therefore, it is reasonable to hypothesize that photocatalytic deposition of Ag^+ onto Pt/TiO_2 would result in core–shell like bimetallic species (Pt@Ag) on the TiO_2 surface, likely giving rise to enhanced ethylene selectivity in the HDC of 1,2-dichloroethane. Thus far, selective HDC of 1,2-dichloroethane on sequentially photodeposited $Pt–Ag/TiO_2$ catalysts has not been reported.

The main objective of this study is to synthesize a novel sequentially photodeposited $Pt–Ag/TiO_2$ catalyst and to test the potential for selective HDC of 1,2-dichloroethane. For comparison, the $Pt–Ag/TiO_2$ catalyst was also prepared using the impregnation method. The catalysts were characterized by X-ray diffraction (XRD), transition electron microscopy (TEM), CO chemisorption, IR spectroscopy of CO adsorption, and X-ray photoelectron spectroscopy (XPS). The catalytic HDC of 1,2-dichloroethane over the catalysts was investigated.

2. Experimental

2.1. Catalyst preparation

To prepare the catalyst, metallic Pt and Ag were sequentially deposited on the TiO_2 surface by photocatalytic reduction. For the preparation of Pt/TiO_2, 2.0 g of TiO_2 (Aeroxide P25, Degussa) was suspended in 480 ml of distilled water containing a required amount of H_2PtCl_6 and 10 ml of methanol. Prior to photodeposition, the suspension was purged by a N_2 flow (60 ml min^{-1}) under stirring for 1 h in the dark. The suspension was then subjected to ultraviolet (UV) irradiation with a high pressure Hg lamp (500 W) for 4 h. The Pt/TiO_2 sample was recovered by filtration, followed by repeated washing with distilled water until neutral and dried at 110 °C for 4 h. The deposition of Ag on Pt/TiO_2 was conducted according to the above described procedure but with $AgNO_3$ as the metal precursor. The resulting bimetallic catalyst was denoted as *pd*-Pt(*x*)–Ag(*y*)/TiO_2, where *x* is the Pt content (wt.%) and *y* is the Ag content (wt.%).

For comparison, the conventional impregnation method was used to prepare supported bimetallic catalysts. A sequential impregnation method was adopted to avoid the precipitation of AgCl [29]. Briefly, TiO_2 was first impregnated with a required amount of $AgNO_3$ solution, followed by drying at 110 °C for 4 h. The resulting material was further impregnated with H_2PtCl_6, followed by drying at 110 °C for 4 h, calcination at 300 °C under air for 4 h, and reduction at 300 °C under H_2 atmosphere for 3 h. The resulting catalyst was denoted as *im*-Pt(*x*)–Ag(*y*)/TiO_2, where *x* is the Pt content (wt.%) and *y* is the Ag content (wt.%).

2.2. Catalyst characterization

XRD patterns of the samples were recorded on a Rigaku D/max-RA powder diffraction-meter (Rigaku, Tokyo, Japan) using Cu Kα radiation. Brunauer–Emmett–Teller (BET) surface areas of the samples were measured using the nitrogen adsorption method on a Micromeritics ASAP 2020 (Micromeritics Instrument Co., Norcross, GA) at −196 °C (77 K). TEM images of the samples were collected on a JEM-200CX electron microscope (JEOL Co., Tokyo, Japan). The UV–vis spectra were obtained in SHIMADZU UV-2450 UV/vis spectrophotometer (Shimadzu Co., Kyoto, Japan) using $BaSO_4$ as a reference. XPS spectra were conducted on a Perkin-Elmer PHI-5000 (ULVAC-PHI Inc., Chigasaki, Japan) equipped with a monochromatized Al Kα X-ray source ($h\nu$ = 1486.6 eV) and a hemispherical electron analyzer. The C 1s peak (284.6 eV) was used for the calibration of binding energy values. The contents of metals in the samples were determined by X-ray fluorescence (ARL-9800) (ARL Co., Switzerland).

CO chemisorption was used to quantify the exposed surface sites of Pt. Typically, the sample was activated at 300 °C in a H_2 flow (40 ml min^{-1}) for 1 h, followed by purging at 300 °C by a He flow (40 ml min^{-1}) for 1 h. After cooling to room temperature, CO chemisorption was performed using the pulse titration mode. CO content in the pulses was determined by an online gas chromatograph (GC) equipped with a thermal conductivity detector (TCD).

CO adsorption on the catalyst samples was measured in a vacuum IR system by a Nicolet 5700 FT-IR spectrometer (ThermoElectron, Madison, US) at 4 cm^{-1} resolution. Briefly, the sample (about 10 mg) was pressed into self-supporting wafer and placed in an IR cell connected to the vacuum system. The sample was activated in H_2 atmosphere by ramping to 300 °C at a rate of 10 °C min^{-1} and holding at the temperature for 2 h. After cooling to room temperature, the sample was exposed to 15 mbar CO for 30 min. After evacuation (<10^{-5} mbar) for 30 min, IR spectra were recorded.

2.3. Catalytic HDC of 1,2-dichloroethane

The gas-phase HDC of 1,2-dichloroethane was conducted in a down-flow glass reactor with a quartz frit at 250 °C under atmospheric pressure. Typically, 100 mg of catalyst was pressed into wafers, sieved to 20–40 mesh, and loaded on a quartz frit. Prior to the catalytic HDC, the catalyst was activated in a H_2 flow (40 ml min^{-1}) at 300 °C for 2 h. After cooling to 250 °C, 1,2-dichloroethane was injected at 0.059 ml h^{-1} into a mixed gas flow (42 ml min^{-1}) using a microprocessor-controlled infusion pump. The gas mixture consisted of 7300 ppm 1,2-dichloroethane, 36,800 ppm H_2, and a balance of He. The reaction products including 1,2-dichloroethane, chloroethane, chloroethylene, ethane and ethylene were analyzed using an online GC equipped with a Porapak Q packed column and a flame-ionization detector (FID).

3. Results and discussion

3.1. Catalyst characterization

The XRD patterns of the samples are shown in Fig. 1S, supporting information. For all samples, diffraction peaks with 2θ of 25.2, 27.6, 37.9, 48.6, 54.1, 55.3 and 62.7° were observed, assigned to the anatase and rutile phases of TiO_2. However, diffraction peaks characteristic of Ag, Pt or Pt–Ag alloy were not identified, likely due to the low content and/or small particle sizes of the metallic species in these samples.

TEM images of the samples are presented in Fig. 1. TiO_2 and surface metal particles could be clearly detected. The particle size of the TiO_2 support varied within 20–50 nm. Given similar metal compositions, the metal particle size of the sample prepared by the sequential photodeposition method was larger than that prepared by the impregnation method. The average metal particle sizes of the catalysts were further quantified on the basis of surface area weighted diameter [21,30] (results summarized in Table 1). The average Pt particle sizes of *pd*-Pt(1.05)/TiO_2 and *im*-Pt(1.06)/TiO_2 were calculated to be 2.6 and 1.9 nm, respectively. The average metal particle size of *im*-Pt–Ag/TiO_2 was nearly identical to that of *im*-Pt(1.06)/TiO_2. For *pd*-Pt–Ag/TiO_2, the average metal particle size was slightly increased with Ag content.

The UV–vis spectra of the different catalysts are compared in Fig. 2. All samples exhibited strong peaks below 400 nm, assigned

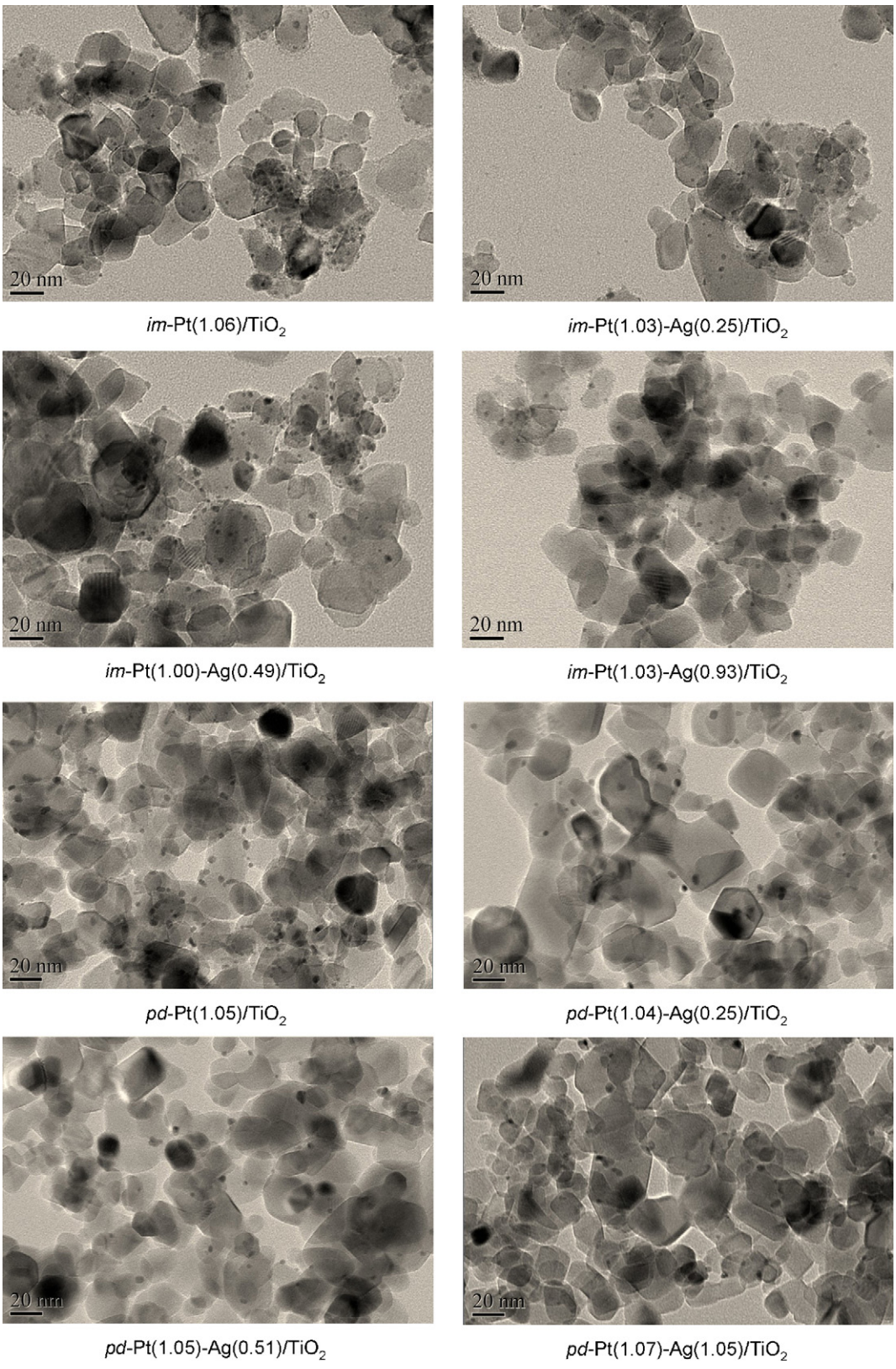

Fig. 1. TEM images of the catalysts.

to the absorbance of anatase and rutile phases of TiO_2 [31]. For *im*-Ag(0.94)/TiO_2, in addition to the absorbance below 400 nm a broad peak was observed around 400–800 nm with a maximum at 490 nm, attributed to the surface plasmon resonance effect of metallic Ag particle [32,33]. As for *pd*-Ag(0.97)/TiO_2, the absorbance characteristic of the plasmon resonance of metallic Ag was identified at 600 nm. The marked red shift of the plasmon resonance absorbance of *pd*-Ag(0.97)/TiO_2 can be ascribed to the larger particle size of Ag, as compared with *im*-Ag(0.94)/TiO_2 [34]. On the contrary, the broad plasmon resonance absorbance was not shown

Table 1
The properties of the catalysts.

Catalyst	Metal loading[a]		Atom ratio	BET surface area	CO adsorption amount	Ag coverage on Pt[b]	Metal particle size[c]	Surface atomic concentration[d]		Ag/Pt
	Pt (wt.%)	Ag (wt.%)	Pt:Ag	(μmol g^{-1})	(m^2 g^{-1})		(nm)	Ag (%)	Pt (%)	
im-Pt(1.06)/TiO_2	1.06	–	–	29.1	52.3	–	1.9 ± 0.2	–	0.31	–
im-Pt(1.03)–Ag(0.25)/TiO_2	1.03	0.25	2.3:1	13.0	51.6	–	2.2 ± 0.3	0.07	0.27	0.26
im-Pt(1.00)–Ag(0.49)/TiO_2	1.00	0.49	1.1:1	5.4	51.9	–	2.2 ± 0.3	0.11	0.25	0.44
im-Pt(1.03)–Ag(0.93)/TiO_2	1.03	0.93	1:1.6	3.1	52.0	–	2.1 ± 0.3	0.21	0.26	0.81
im-Ag(0.94)/TiO_2	–	0.94	0	–	–	–	–	–	–	–
pd-Pt(1.05)/TiO_2	1.05	–	–	22.6	50.2	–	2.6 ± 0.3	–	0.21	–
pd-Pt(1.04)–Ag(0.25)/TiO_2	1.04	0.25	2.3:1	1.1	52.5	0.95	2.7 ± 0.3	0.18	0.20	0.90
pd-Pt(1.05)–Ag(0.51)/TiO_2	1.05	0.51	1.1:1	0.9	50.9	0.96	3.1 ± 0.3	0.21	0.21	1.00
pd-Pt(1.07)–Ag(1.05)/TiO_2	1.07	1.05	1:1.8	0.7	52.1	0.97	3.5 ± 0.4	0.37	0.19	1.95
pd-Ag(0.97)/TiO_2	–	0.97	0	–	–	–	–	–	–	–

[a] Determined by X-ray fluorescence.
[b] Determined by CO adsorption.
[c] Calculated from transition electron microscopy.
[d] Determined by X-ray photoelectron spectroscopy.

on *im*-Pt–Ag/TiO_2, reflecting the absence of metallic Ag domain on the TiO_2 surface. The results imply the formation of Pt–Ag ensemble with well mixed Pt and Ag atoms. The plasmon resonance absorbance of Ag was also distinct on *pd*-Pt–Ag/TiO_2, suggesting the presence of metallic Ag domain. Site specific growth of Ag on Pt/TiO_2 during the process of photodeposition facilitated the formation of core–shell like bimetallic species (Pt@Ag). In comparison with *pd*-Pt(0.97)/TiO_2, *pd*-Pt–Ag/TiO_2 displayed a blue shift in the plasmon resonance absorbance. For *pd*-Pt–Ag/TiO_2, increasing Ag content led to a significant red shift of the plasmon resonance absorbance, indicative of an increased size of the metallic Ag domain with Ag content.

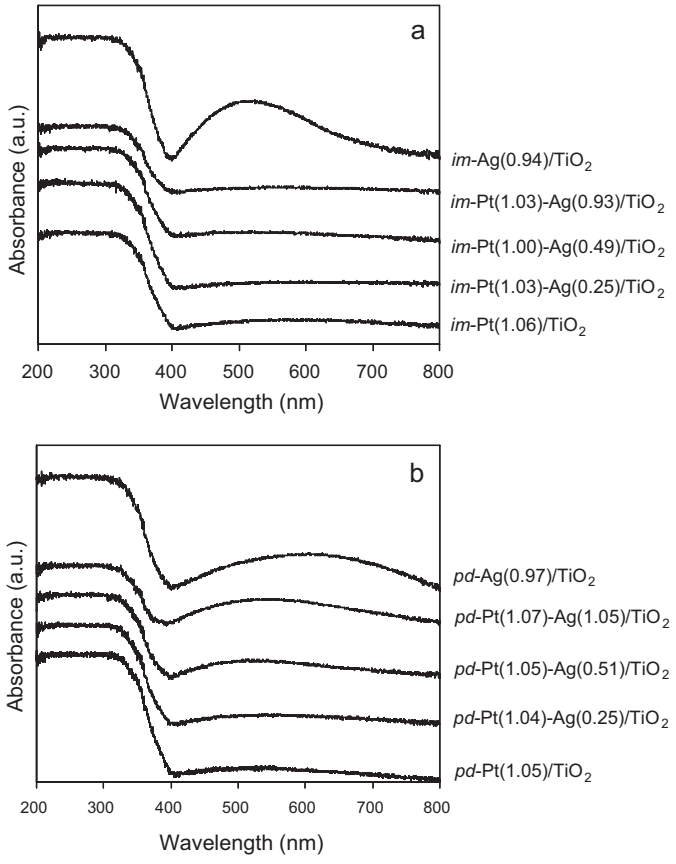

Fig. 2. UV–vis spectra of the samples prepared by (a) impregnation and (b) sequential photodeposition method.

The superficial metal compositions of the catalysts from the XPS analysis are summarized in Table 1. The surface atomic concentration of metallic Pt was 0.21% for *pd*-Pt(1.05)/TiO_2 and was 0.31% for *im*-Pt(1.06)/TiO_2, reflecting the higher Pt dispersion and smaller Pt particle sizes of *im*-Pt(1.06)/TiO_2, in agreement with the TEM observation. For the bimetallic catalysts, given similar metal compositions larger Ag/Pt surface atomic ratios were observed on *pd*-Pt–Ag/TiO_2 than on *im*-Pt–Ag/TiO_2, indicating higher surface Ag enrichment of *pd*-Pt–Ag/TiO_2. For example, the surface Ag/Pt ratio was 0.26 for *im*-Pt(1.03)–Ag(0.25)/TiO_2, but 0.90 for *pd*-Pt(1.04)–Ag(0.25)/TiO_2. For *pd*-Pt–Ag/TiO_2, the sequential photodeposition of metallic Ag on Pt/TiO_2 led to preferential growth of metallic Ag domain on the surface of Pt particles and thus to the formation of core–shell like bimetallic species (Pt@Ag). On the other hand, for *im*-Pt–Ag/TiO_2 well mixed Pt–Ag ensemble was formed. Hence, higher surface Ag enrichment was shown on *pd*-Pt–Ag/TiO_2 than on *im*-Pt–Ag/TiO_2 at similar metal compositions.

The higher surface Ag enrichment in *pd*-Pt–Ag/TiO_2 was further verified by the results of CO chemisorption (presented in Table 1). Because metallic Ag is incapable of adsorbing CO [35,36], the chemisorbed concentration of CO would only correlate to the exposed Pt sites of the catalyst. The chemisorbed concentration of CO was higher on *im*-Pt(1.06)/TiO_2 (29.1 μmol g^{-1}) than on *pd*-Pt(1.05)/TiO_2 (22.6 μmol g^{-1}). For *im*-Pt–Ag/TiO_2, as the Ag content increased from 0.25 to 0.93 wt.%, the chemisorbed concentration of CO decreased markedly from 13.0 to 3.1 μmol g^{-1}, reflecting the lowered exposure of Pt sites by Ag addition. It is worth noting that all *im*-Pt–Ag/TiO_2 catalysts had similar metal particle sizes (see Table 1). The observed negative correlation between the exposure of Pt sites and the Ag content in *im*-Pt–Ag/TiO_2 can be explained by the dilution effect [9,10,13,14] of Ag. Much more pronounced adsorption suppression of CO by the Ag content was shown on *pd*-Pt–Ag/TiO_2 than on *im*-Pt–Ag/TiO_2. Compared with *pd*-Pt(1.05)/TiO_2, the chemisorbed CO amount of *pd*-Pt(1.07)–Ag(1.05)/TiO_2 decreased to 0.7 μmol g^{-1}. Because *pd*-Pt–Ag/TiO_2 has approximately identical Pt particles, the coverage of Ag on Pt can be further estimated, and the results are listed in Table 1. The Ag coverages were 0.95, 0.96 and 0.97 for *pd*-Pt(1.04)–Ag(0.25)/TiO_2, *pd*-Pt(1.05)–Ag(0.51)/TiO_2, and *pd*-Pt(1.07)–Ag(1.05)/TiO_2, respectively, reflecting effective blockage of the exposed Pt sites by metallic Ag. Notably, increasing Ag content from 0.25 to 1.05 wt.% only leads to slightly increased Ag coverage, indicating that Ag is deposited first on Pt surface and subsequently on Ag surface.

The IR spectra of CO adsorption on the catalysts are compiled in Fig. 3. For both *pd*-Ag(0.97)/TiO_2 and *im*-Ag(0.94)/TiO_2, IR bands characteristic of CO adsorption were not identified, reflecting

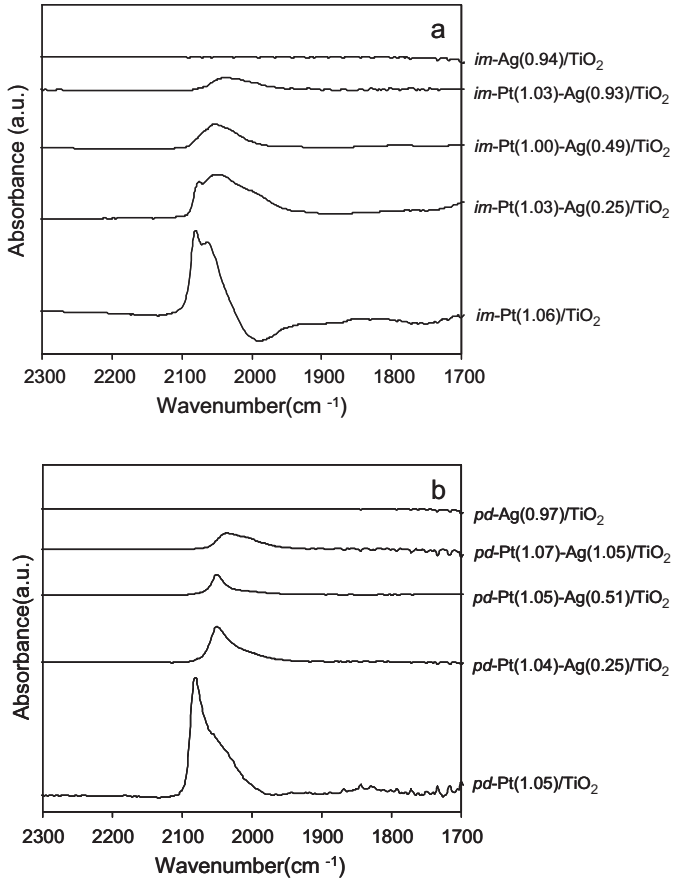

Fig. 3. IR spectra of CO adsorption on the catalysts prepared by (a) impregnation and (b) sequential photodeposition method.

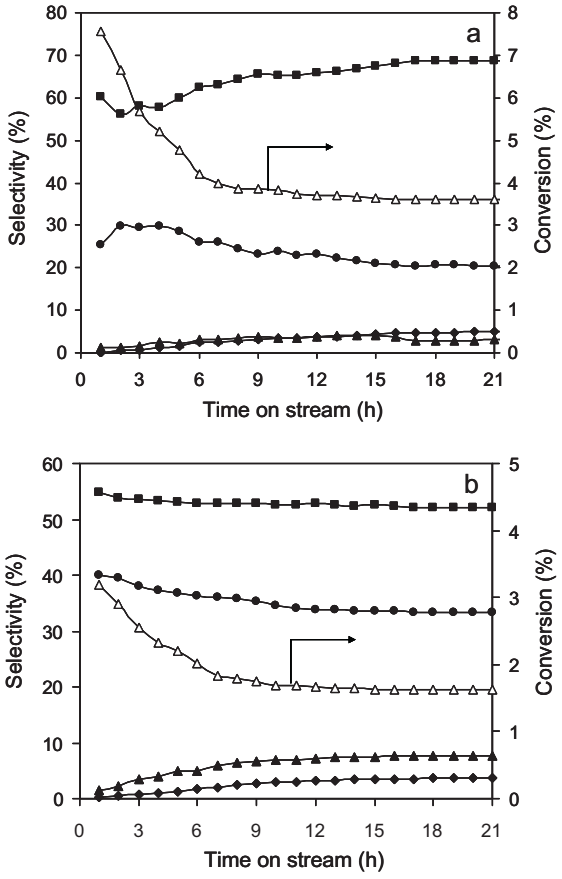

Fig. 4. The HDC of 1,2-dichloroethane over (a) *im*-Pt(1.06)/TiO_2 and (b) *pd*-Pt(1.05)/TiO_2 as a function of time on stream. (♦) Ethylene; (■) ethane; (▲) chloroethylene; (●) chloroethane; and (△) conversion.

the absence of chemisorbed CO on the surface of metallic Ag [35,36]. As for *pd*-Pt(1.05)/TiO_2, a strong band at 2082.8 cm^{-1} with a shoulder around 2050 cm^{-1}, and a weak band around 1840 cm^{-1} were observed, respectively, assigned to the linear and bridged CO adsorption [37,38]. The multiple bands observed within 2000–2100 cm^{-1} were characteristic of linear CO adsorption on different Pt sites, e.g. plane and defect sites (edges and corners) [39–41]. Compared with the plane sites, CO adsorption on the defect sites is expected to induce marked blue-shifts due to the stronger adsorptive interaction [42]. Hence, the IR bands at 2082.8 and 2050 cm^{-1} can be assigned to CO adsorption on the plane sites and defect sites of metallic Pt particles, respectively. For *im*-Pt(1.06)/TiO_2, the IR bands observed at 2080.9 and 2063.6 cm^{-1} can be assigned to the linear CO adsorption on the plane and defects sites, respectively. When compared with *pd*-Pt(1.05)/TiO_2, *im*-Pt(1.06)/TiO_2 displayed stronger bands associated with the defect sites, suggesting that more defect sites existed on the surface of Pt particles, likely resulting from their smaller sizes [41].

Very different IR spectra were shown on the bimetallic catalysts. For both *pd*-Pt–Ag/TiO_2 and *im*-Pt–Ag/TiO_2, the band intensities decreased with the Ag content and were lower than their respective monometallic Pt catalysts, indicative of less exposed Pt sites. For *pd*-Pt–Ag/TiO_2, only IR bands within the range of 2054–2045 cm^{-1} reflecting the linear CO adsorption were observed. The absence of the band around 1840 cm^{-1} characteristic of the bridged CO adsorption implies no presence of adjacent Pt sites in *pd*-Pt–Ag/TiO_2. Moreover, the IR band at 2084 cm^{-1} characteristic of CO adsorption on the plane sites was negligible. Similar results were observed by Schaal et al. [43]. Provided that photodeposition of metallic Ag on *pd*-Pt/TiO_2 did not change the structure of Pt particles, it can be derived that metallic Ag preferentially deposited on the plane sites of Pt particles, and consequently blocked these sites from CO adsorption. It should be emphasized that the plane sites are dominated by adjacent Pt atoms, while the defect sites are dominated by small and discrete Pt ensemble. Thus, it can be concluded that the majority of the exposed Pt ensembles on *pd*-Pt–Ag/TiO_2 were small and discrete upon Ag deposition. As for *im*-Pt–Ag/TiO_2, the IR band gradually red shifted and the intensity also decreased with the Ag content. For *im*-Pt–Ag/TiO_2, Pt was diluted by Ag to form a well mixed Pt–Ag ensemble; therefore, the increase of Ag content led to decreased CO adsorption and to suppressed dipole–dipole interaction between neighbor adsorbed CO molecules, giving rise to gradually red-shifted IR bands [10,14]. Alternatively, the electronic effects between Ag and Pt in the bimetallic ensemble also accounted for the red-shifted of CO adsorption [44].

3.2. Catalytic hydrodechlorination of 1,2-dichloroethane

The activities and selectivities of *pd*-Pt(1.05)/TiO_2 and *im*-Pt(1.06)/TiO_2 for the HDC of 1,2-dichloroethane as a function of time on stream (TOS) are compiled in Fig. 4. For Ag/TiO_2 prepared by either the impregnation method or the photodeposition method, negligible 1,2-dichloroethane conversion was identified (results not shown), ascribed to the rapid and irreversible deactivation of Ag sites by chlorine during the HDC process [16]. On the other hand, effective dechlorination of 1,2-dichloroethane was achieved on the Pt containing monometallic and bimetallic catalysts, reflecting the curial role of Pt in H_2 activation.

For *pd*-Pt(1.05)/TiO_2 and *im*-Pt(1.06)/TiO_2, besides chloroethane and chloroethylene, a series of completely dechlorinated products (C1–C4 hydrocarbons) were detected with ethane as the predominant one. The steady state ethylene selectivity was 5.0% for *pd*-Pt(1.05)/TiO_2 and 3.6% for *im*-Pt(1.06)/TiO_2. The observed low ethylene selectivity can be mainly ascribed to the strong ability of Pt in H_2 activation and ethylene adsorption due to the presence of adjacent Pt sites [10,14]. The intermediate product ethylene was strongly adsorbed on the adjacent Pt sites to form a di-δ-complex [14,45], and thus was susceptible to further hydrogenation to ethane. Moreover, the 1,2-dichloroethane conversion gradually decreased at early TOS, reflecting declined activities of the catalysts due to strong HCl adsorption, coke deposition on the Pt surface, and/or Pt particle aggregation during the HDC process [46–48]. Furthermore, resulting from the smaller particle size and more defect sites of Pt, *im*-Pt(1.06)/TiO_2 showed much higher initial and steady-state activities than *pd*-Pt(1.05)/TiO_2.

The catalytic activity of *im*-Pt–Ag/TiO_2 was lower than that of *im*-Pt(1.06)/TiO_2. Moreover, increasing Ag content led to decreased initial and steady-state activities of *im*-Pt–Ag/TiO_2, likely due to the decreased content of exposed Pt sites with Ag content (see Table 1). Compared with *im*-Pt(1.06)/TiO_2, *im*-Pt–Ag/TiO_2 displayed substantially enhanced ethylene selectivity (results presented in Fig. 5). After 28 h on stream, the ethylene selectivity was 17.8% for *im*-Pt(1.03)–Ag(0.25)/TiO_2, 48.1% for *im*-Pt(1.00)–Ag(0.49)/TiO_2, and 68.1% for *im*-Pt(1.03)–Ag(0.93)/TiO_2, indicative of enhanced ethylene selectivity with the Ag content. The Ag content dependent ethylene selectivity can be well interpreted in terms of the ensemble effect [10–19,49]. In principle, the catalytic HDC of 1,2-dichloroethane over bimetallic catalysts is commenced with dissociative adsorption of 1,2-dichloroethane on the metal surface. Due to the strong adsorption on the surface Ag sites, 1,2-dichloroethane is preferentially dechlorinated to ethylene, leaving the surface Ag sites deactivated by chlorine. The resulting AgCl is feasibly reduced into metallic Ag by active H provided by the vicinal Pt sites [10,16]. For *im*-Pt–Ag/TiO_2, the bimetallic species formed a well mixed Pt–Ag ensemble, and small and discrete Pt ensembles were formed due to surface Ag dilution. As a result, small and discrete Pt ensembles gradually dominated with the increase of Ag content at the expense of adjacent Pt sites, as reflected by the results of CO chemisorption and CO adsorption IR. Because effective adsorption and further hydrogenation of ethylene to ethane only occur on adjacent Pt sites [14], the discrete Pt ensembles are too small to effectively catalyze the hydrogenation of adsorbed ethylenic species from 1,2-dichloroethane dechlorination on Ag sites to ethane. Hence, the decrease of adjacent Pt sites would increase the ethylene selectivity. Therefore, enhanced ethylene selectivity was achieved with the increase of Ag content in *im*-Pt–Ag/TiO_2.

It is worthy to note that all *im*-Pt–Ag/TiO_2 catalysts exhibited distinct transient behavior at early TOS – the conversion of 1,2-dichloroethane decreased, while the ethylene selectivity increased. Different metallic species including both discrete and adjacent Pt and Ag sites might exist in *im*-Pt–Ag/TiO_2. The rapid decrease of 1,2-dichloroethane conversion at early TOS can be primarily ascribed to the deactivation of adjacent Pt sites, as evidenced by the similar deactivation trend of *im*-Pt(1.06)/TiO_2. With the increasing Ag content, the contribution to 1,2-dichloroethane conversion from the surface Ag sites gradually increased, consequently leading to enhanced ethylene selectivity. Moreover, the surface Ag enrichment might occur in a Pt–Ag ensemble during the HDC reaction [12,20]. This helps to explain the gradually enhanced ethylene selectivity with the proceeding of the HDC.

The catalytic behavior of *pd*-Pt–Ag/TiO_2 is displayed in Fig. 6. Moderate deactivation at early TOS was observed on *pd*-Pt(1.04)–Ag(0.25)/TiO_2, and slight deactivation was observed

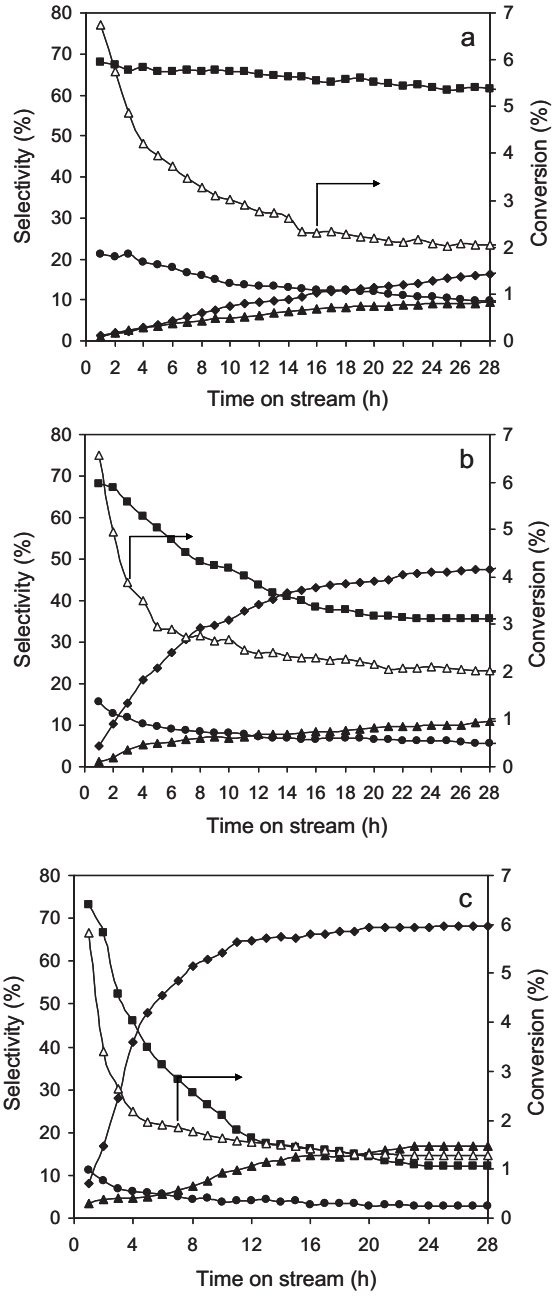

Fig. 5. The HDC of 1,2-dichloroethane over (a) *im*-Pt(1.03)–Ag(0.25)/TiO_2 and (b) *im*-Pt(1.00)–Ag(0.49)/TiO_2 and (c) *im*-Pt(1.03)–Ag(0.93)/TiO_2 as a function of time on stream. (♦) Ethylene; (■) ethane; (▲) chloroethylene; (●) chloroethane; and (△) conversion.

on other *pd*-Pt–Ag/TiO_2, indicative of much higher catalytic stability when compared with *im*-Pt–Ag/TiO_2. The high catalytic stability of *pd*-Pt–Ag/TiO_2 was further reflected by the stable and TOS independent ethylene selectivity during the HDC process. Notably, at early TOS trace ethane (<0.42%) was detected on *pd*-Pt(1.04)–Ag(0.25)/TiO_2, but not on other *pd*-Pt–Ag/TiO_2. The lower catalytic stability and ethylene selectivity observed on *pd*-Pt(1.04)–Ag(0.25)/TiO_2 can be ascribed to the incomplete blocking of the exposed adjacent Pt sites due to insufficient deposited Ag. In contrast, the Ag content in *pd*-Pt(1.05)–Ag(0.51)/TiO_2 or *pd*-Pt(1.07)–Ag(1.05)/TiO_2 was high enough to sufficiently block the adjacent Pt sites. Nonetheless, given the similar bimetallic compositions, *pd*-Pt–Ag/TiO_2 exhibited much higher ethylene selectivity than *im*-Pt–Ag/TiO_2–74.3% for

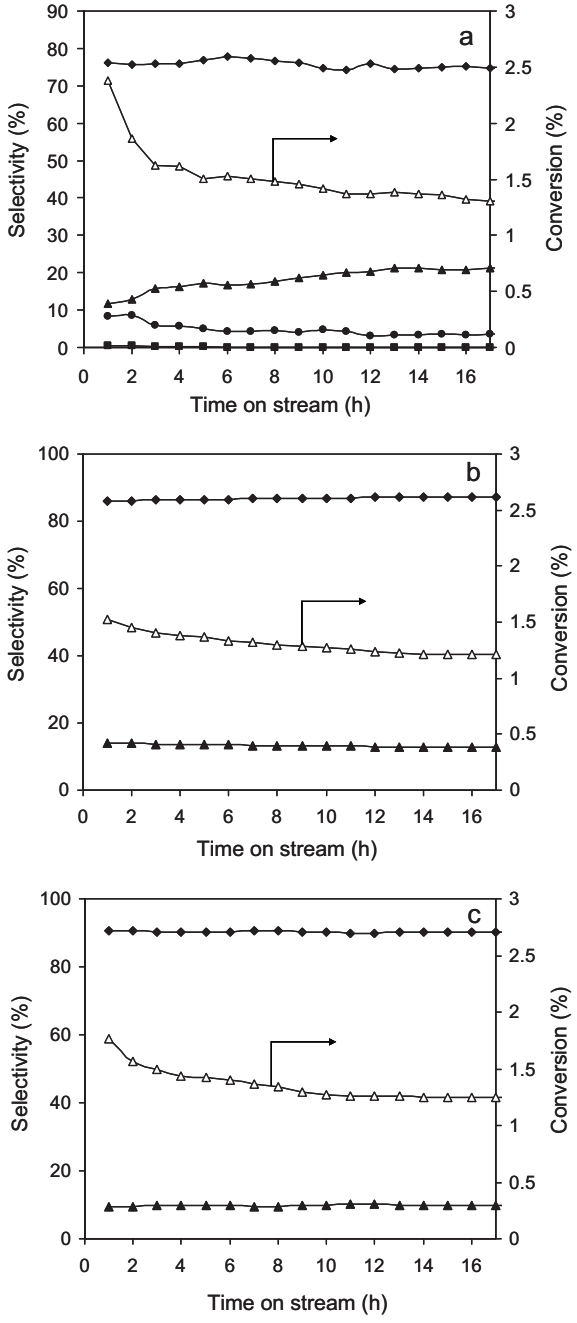

Fig. 6. The HDC of 1,2-dichloroethane over (a) *pd*-Pt(1.04)–Ag(0.25)/TiO_2 and (b) *pd*-Pt(1.05)–Ag(0.51)/TiO_2 and (c) *pd*-Pt(1.07)–Ag(1.05)/TiO_2 as a function of time on stream. (♦) Ethylene; (■) ethane; (▲) chloroethylene; (●) chloroethane; and (△) conversion.

pd-Pt(1.04)–Ag(0.25)/TiO_2, 87.1% for *pd*-Pt(1.05)–Ag(0.51)/TiO_2, and 90.0% for *pd*-Pt(1.07)–Ag(1.05)/TiO_2.

The very high catalytic stability and ethylene selectivity of *pd*-Pt–Ag/TiO_2 can be attributed to the site specific growth of Ag domain on the surface of Pt particles. In such a fashion, adjacent Pt sites were effectively blocked by a relatively low content of Ag. Characterization results revealed that given approximately 1.0 wt.% of Pt, 0.25 wt.% of Ag could nearly completely block the plane sites of Pt, leaving only 4.9% of the Pt sites exposed. Hence, for *pd*-Pt–Ag/TiO_2 the dissociative dechlorination occurred predominantly on the surface Ag sites, while the exposed Pt sites were mainly responsible for the dissociative activation of H_2 to regenerate the deactivated surface Ag sites. Due to the very low content of exposed Pt sites in *pd*-Pt–Ag/TiO_2, most surface Ag sites are expected to locate away from the exposed Pt sites. Xie et al. [10] found that the deactivated Cu sites in Pd–Cu/SiO_2 could be effectively regenerated by the neighbor Pd sites during the HDC of 1,2-dichloroethane. In parallel, Sa and Vinek [50] investigated the catalytic hydrogenation of nitrate over Pd–Cu/Al_2O_3, and concluded that the deactivated Cu sites could be more readily regenerated by the neighbor Pd sites than by the spilled over hydrogen through the support. Despite the different Ag contents, the steady state 1,2-dichloroethane conversions were nearly identical on *pd*-Pt(1.04)–Ag(0.25)/TiO_2 (1.3%), *pd*-Pt(1.05)–Ag(0.51)/TiO_2 (1.2%), and *pd*-Pt(1.07)–Ag(1.05)/TiO_2 (1.2%), indicating that the catalytic activity was independent on the Ag content in the experimental setting. It is well documented that H_2 can effectively permeate through noble metal membranes via a solution-diffusion transport mechanism [51,52]. Although the content of exposed Pt sites in *pd*-Pt–Ag/TiO_2 was low, the activated H_2 could penetrate the Pt core to access the upper Ag sites, and as a result the deactivated Ag sites were effectively regenerated.

4. Conclusions

Pt–Ag/TiO_2 catalysts were prepared by the sequential photodeposition and impregnation methods, and the catalytic HDC of 1,2-dichloroethane over the catalysts was investigated. UV–vis results show that a metallic Ag domain presents on the surface of Pt particles in *pd*-Pt–Ag/TiO_2, attributed to the site specific deposition of Ag on the Pt surface to form a core–shell (Pt@Ag) like structure. Alternatively, Pt–Ag ensemble is predominant in *im*-Pt–Ag/TiO_2. Given similar Ag loading levels, *pd*-Pt–Ag/TiO_2 displays higher surface Ag enrichment than *im*-Pt–Ag/TiO_2. In parallel, the chemisorbed concentration of CO is much lower on *pd*-Pt–Ag/TiO_2 than on *im*-Pt–Ag/TiO_2, suggesting effective surface blocking of the exposed Pt sites by the photodeposited Ag. Accordingly, much more stable catalytic stability and enhanced ethylene selectivity are shown on *pd*-Pt–Ag/TiO_2. For comparison, *im*-Pt–Ag/TiO_2 exhibits a distinct transient behavior, where the ethylene selectivity increases with TOS at the expense of 1,2-dichloroethane conversion.

Acknowledgements

The financial support from the Natural Science Foundation of China (Nos. 21107043 and 20877039), Program of New Century Excellent Talents in University (NECT-08-0277), the Natural Science Foundation of Jiangsu Province, China (Nos. BK2010378 and BK2010051) and Special of Foundation for the Doctor-subject of China (No. 20100091120016) are gratefully acknowledged. We are indebted to the Modern Analytical Center, Nanjing University for the catalyst characterization.

Appendix A. Supplementary data

Supplementary data associated with this article can be found, in the online version, at http://dx.doi.org/10.1016/j.apcatb.2012.05.016.

References

[1] T.M. Vogel, C.S. Criddle, P.L. McCarty, Environmental Science and Technology 21 (1987) 722–736.
[2] M. Tancrede, R. Wilson, L. Zeise, E.A.C. Crouch, Atmospheric Environment 21 (1987) 2187–2205.
[3] E. Goldberg, Science of the Total Environment 100 (1991) 17–28.
[4] H.R. Bauser, Chemosphere 8 (1979) 415–424.
[5] T.N. Kalnes, R.B. James, Environmental Progress 7 (1988) 185–191.
[6] M. Bonarowska, Z. Kaszkur, L. Kępiński, Z. Karpiński, Applied Catalysis B: Environmental 99 (2010) 248–256.

[7] Z.M. de Pedro, J.A. Casas, L.M. Comez-Sainero, J.J. Rodriguez, Applied Catalysis B: Environmental 98 (2010) 79–85.
[8] B.T. Meshesha, R.J. Chimentão, A.M. Segarra, J. Llorca, F. Medina, B. Coq, J.E. Sueiras, Applied Catalysis B: Environmental 105 (2011) 361–372.
[9] L. Li, X.D. Wang, A.Q. Wang, J.Y. Shen, T. Zhang, Thermochimica Acta 494 (2009) 99–103.
[10] H. Xie, J.Y. Howe, V. Schwartz, J.R. Monnier, C.T. Williams, H.J. Ploehn, Journal of Catalysis 259 (2008) 111–122.
[11] S. Lambert, F. Ferauche, A. Brasseur, J.-P. Pirard, B. Heinrichs, Catalysis Today 100 (2005) 283–289.
[12] W.D. Rhodes, J.L. Margitfalvi, I. Borbath, K. Lazar, V.I. Kovalchuk, J.L. d'Itri, Journal of Catalysis 230 (2005) 86–97.
[13] L.S. Vadlamannati, V.I. Kovalchuk, J.L. d'Itri, Catalysis Letters 58 (1999) 173–178.
[14] V.Y. Borovkov, D.R. Luebke, V.I. Kovalchuk, J.L. d'Itri, Journal of Physical Chemistry B 107 (2003) 5568–5574.
[15] B. Heinrichs, J.P. Schoebrechts, J.P. Pirard, Journal of Catalysis 200 (2001) 309–320.
[16] B. Heinrichs, P. Delhez, J.P. Schoebrechts, J.P. Pirard, Journal of Catalysis 172 (1997) 322–335.
[17] B. Heinrichs, F. Noville, J.P. Schoebrechts, J.P. Pirard, Journal of Catalysis 220 (2003) 215–225.
[18] B. Heinrichs, F. Noville, J.P. Schoebrechts, J.P. Pirard, Journal of Catalysis 192 (2000) 108–118.
[19] A. Srebowata, W. Lisowski, J.W. Sobczak, Z. Karpinski, Catalysis Today 175 (2011) 576–584.
[20] D.R. Luebke, L.S. Vadlamannati, V.I. Kovalchuk, J.L. d'Itri, Applied Catalysis B: Environmental 35 (2002) 211–217.
[21] H. Chen, Y. Shao, Z.Y. Xu, H.Q. Wan, Y.Q. Wan, S.R. Zheng, D.Q. Zhu, Applied Catalysis B: Environmental 105 (2011) 255–262.
[22] S. Hwang, M.C. Lee, W.Y. Choi, Applied Catalysis B: Environmental 46 (2003) 49–63.
[23] S.C. Chan, M.A. Barteau, Langmuir 21 (2005) 5588–5595.
[24] J.M. Herrmann, Catalysis Today 53 (1999) 115–129.
[25] M.R. Hoffmann, S.T. Martin, W. Choi, D.W. Bahnemann, Chemical Reviews 95 (1995) 69–96.
[26] A.L. Linsebigler, G.Q. Lu, J.T. Yates, Chemical Reviews 95 (1995) 735–758.
[27] C. Young, T.M. Lim, K. Chiang, J. Scott, R. Amal, Applied Catalysis B: Environmental 78 (2008) 1–10.
[28] T.A. Egerton, J.A. Mattinson, Applied Catalysis B: Environmental 99 (2010) 407–412.
[29] P.P. Kulkarni, V.I. Kovalchuk, J.L. d'Itri, Applied Catalysis B: Environmental 36 (2002) 299–309.
[30] H. Chen, Z.Y. Xu, H.Q. Wan, J.Z. Zheng, D.Q. Yin, S.R. Zheng, Applied Catalysis B: Environmental 96 (2010) 307–313.
[31] Q.H. Zhang, L. Gao, J.K. Guo, Applied Catalysis B: Environmental 26 (2000) 207–215.
[32] H.M. Coleman, K. Chiang, R. Amal, Chemical Engineering Journal 113 (2005) 65–72.
[33] H. Zhang, G. Wang, D. Chen, X.J. Lv, J.H. Li, Chemistry of Materials 20 (2008) 6543–6549.
[34] K. Matsubara, K.L. Kelly, N. Sakaia, T. Tatsuma, Journal of Materials Chemistry 19 (2009) 5526–5532.
[35] Y. Soma-Noto, W.M.H. Sachtler, Journal of Catalysis 32 (1974) 315–324.
[36] D. Cormack, J. Pritchard, R.L. Moss, Journal of Catalysis 37 (1975) 548–552.
[37] R.P. Eischens, W.A. Pliskin, Advances in Catalysis 10 (1958) 1–56.
[38] R. Barth, R. Pitchai, R.L. Anderson, X.E. Verykios, Journal of Catalysis 116 (1989) 61–70.
[39] R.G. Greenler, K.D. Burch, K. Kretzschar, R. Klauser, A.M. Bradshaw, Surface Science 152–153 (1985) 336–345.
[40] X.L. Zhu, Y.B. Xie, C.J. Liu, Y.P. Zhang, Journal of Molecular Catalysis A: Chemical 282 (2008) 67–73.
[41] M.J. Lundwall, S.M. McClure, D.W. Goodman, Journal of Physical Chemistry C 114 (2010) 7904–7912.
[42] H. Song, R.M. Rioux, J.D. Hoefelmeyer, R. Komor, K. Niesz, M. Grass, P. Yang, G.A. Somorjai, Journal of the American Chemical Society 128 (2006) 3027–3037.
[43] M.T. Schaal, A.C. Pickerell, C.T. Williams, J.R. Monnier, Journal of Catalysis 254 (2008) 131–143.
[44] O. Rosseler, A. Louvet, V. Keller, N. Keller, Chemical Communications 47 (2011) 5331–5333.
[45] R.D. Cortright, J.A. Dumesic, Journal of Catalysis 148 (1994) 771–778.
[46] B. Coq, G. Ferrat, F. Figueras, Journal of Catalysis 101 (1986) 434–445.
[47] A. Wiersma, E.J.A.X. van de Sandt, M.A. den Hollander, H. Van Bekkum, M. Makkee, J.A. Moulijn, Journal of Catalysis 177 (1998) 29–39.
[48] A. Gampine, D.P. Eyman, Journal of Catalysis 179 (1998) 315–325.
[49] W.D. Rhodes, K. Lázár, V.I. Kovalchuk, J.L. d'Itri, Journal of Catalysis 211 (2002) 173–182.
[50] J. Sa, H. Vinek, Applied Catalysis B: Environmental 57 (2005) 247–256.
[51] V.M. Gryaznov, V.I. Vedernikov, S.G. Gulyanova, Kinetika i Kataliz 27 (1986) 142–149.
[52] S. Uemiya, M. Kajiwara, T. Kojima, AIChE Journal 43 (1997) 2715–2723.